Electronic Supplementary Material (ESI) for Journal of Materials Chemistry C.
This journal is © The Royal Society of Chemistry 2024

A low power flexible halide perovskite-based threshold switching memristor as an artificial nociceptor

Lingzhi Tang[a], Jiaan Wang[a], Yang Huang[a], Hengshan Wang[a], Chen Wang[*b], and Yiming Yang[*a]

a. School of Microelectronics, Dalian University of Technology, Dalian Liaoning 116024, China.

b. School of Microelectronics, Fudan University, Shanghai 200433, China. E-mail: chen_w@fudan.edu.cn

Table. S1 The comparison of V_{th}, I_{cc}, I_{off}, P_s and P_o of other TS memristors.

Device	V_{th}	I_{CC}	I_{off}	Ps	P_O	References
W/MgO/Mg/W	1 V	100 μA	10^{-9} A	10^{-11} W	10^{-4} W	1
s-ITO/c-ITO/PET	3.3 V	100 μA	10^{-9} A	10^{-11} W	10^{-4} W	2
W/VO_2/Pt	0.4 V	10 mA	10^{-4} A	10^{-6} W	10^{-3} W	3
Ag/MnO_2/Ag	3 V	10 μA	10^{-9} A	10^{-11} W	10^{-5} W	4
Ag/ZrO_2/Pt	0.25 V	10 μA	10^{-9} A	10^{-11} W	10^{-6} W	5
Ag/SiO_x/W	0.3 V	100 uA	10^{-10} A	10^{-12} W	10^{-5} W	6
Pt/HfO_2/GO/ITO	2.5 V	10 mA	10^{-6} A	10^{-8} W	10^{-2} W	7
Cu/GeTe/Al_2O_3/Pt	0.7 V	50 μA	10^{-7} A	10^{-9} W	10^{-6} W	8
TiN/TiO_2/NbO_X/Pt	1.3 V	1 mA	10^{-6} A	10^{-8} W	10^{-3} W	9
Cu/TaO_x/d-Cu/Pt	0.2 V	10 μA	10^{-9} A	10^{-11} W	10^{-6} W	10
Ag/a-LSMO/Pt	0.45 V	1 uA	10^{-9} A	10^{-11} W	10^{-7} W	11
Pt/Ag:SiO_xN_y/Ti	1.5 V	100 uA	10^{-9} A	10^{-11} W	10^{-4} W	12
Ag/TiO_2/Pt/Ti/SiO_2/Si	0.7 V	5 μA	10^{-8} A	10^{-10} W	10^{-7} W	13
Ag/ZrO_x/Pt	0.4 V	10 nA	10^{-10}A	10^{-12} W	10^{-9} W	14
Ag/FK-800/Pt	3 V	10 μA	10^{-10}A	10^{-12} W	10^{-5} W	15
Au/Ag NW–P(VDF-HFP)/Au	0.25 V	1 μA	10^{-9} A	10^{-11} W	10^{-8} W	16
Au/Ag/PMMA/OIHP:Ag/ITO	0.2 V	0.1 μA	10^{-11} A	10^{-13} W	10^{-8} W	This work

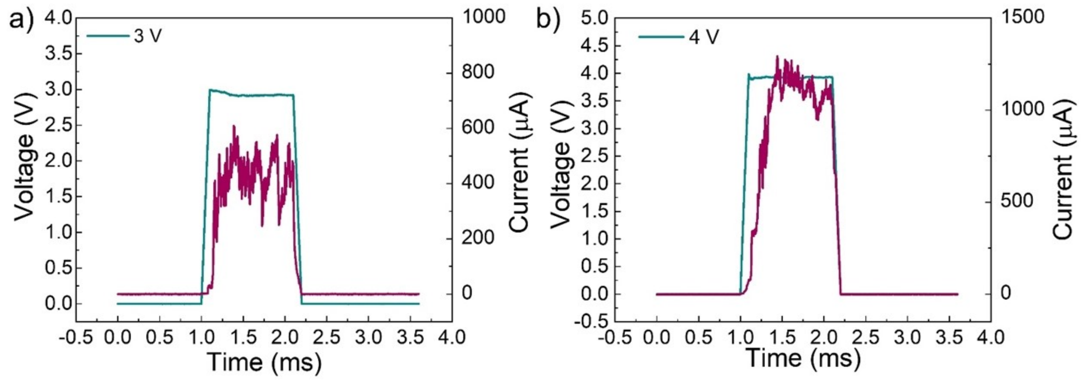

Fig. S1 The harmful stimulations of a single stress pulse with the amplitude of a) 3 V and b) 4 V, the pulse width is 1 ms. The purple curve is the corresponding response current.

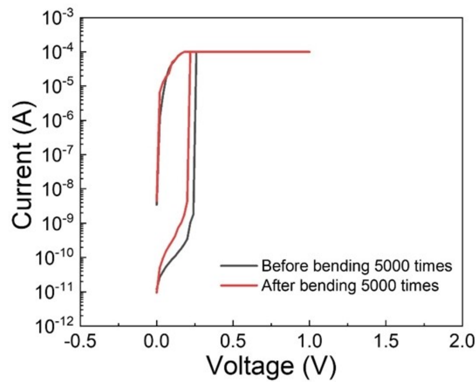

Fig. S2 The I-V curves of Au/Ag/PMMA/OIHP:Ag/ITO device before and after bending 5000 times.

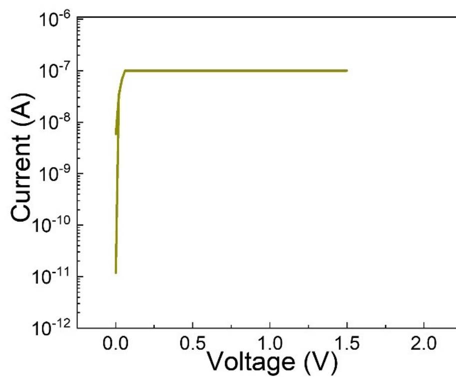

Fig. S3 The I-V curve of TS memristor without PMMA protective layer at 80% humidity after 48 h.

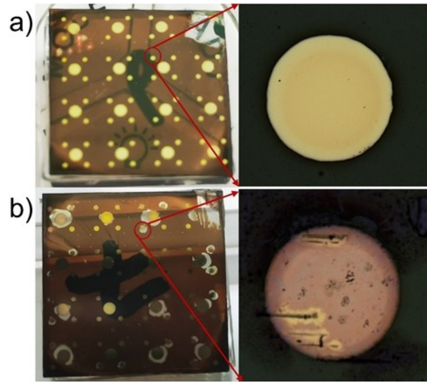

Fig. S4 The microscope morphologies of the devices: a) without and b) with PMMA protective layer at 80% humidity after 48 h.

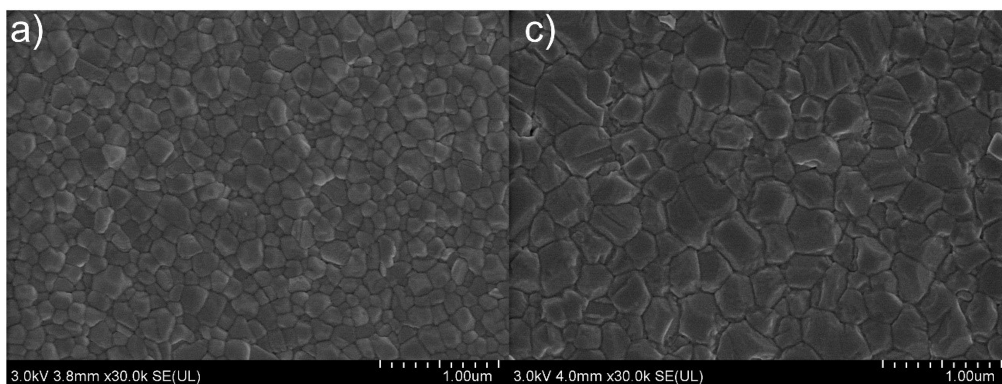

Fig. S5 The SEM morphologies of a) pure OIHP film and b) OIHP:Ag film.

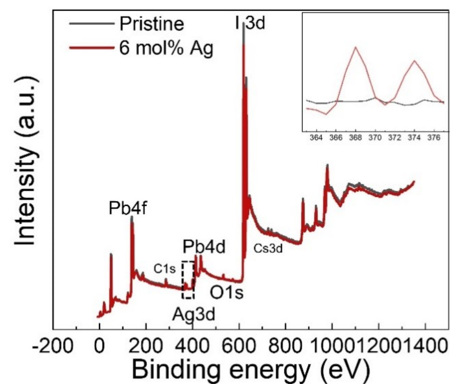

Fig. S6 The X-ray photoelectron spectroscopy (XPS) spectrum of OIHP film and OIHP:Ag film, the upper right corner is the enlarged image of black box of the Ag element. It can be clearly observed from the enlarged image that there is no Ag element related peak in OIHP film. But the XPS energy spectrum of OIHP: Ag film shows Ag related peak, this indicates that Ag was successfully doped into OIHP thin films.

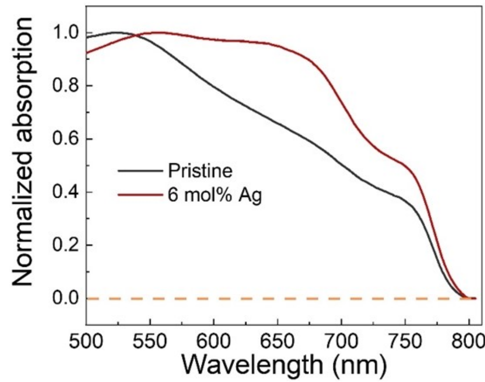

Fig. S7 The optical UV-vis absorption spectra of pure OIHP films and OIHP:Ag films.

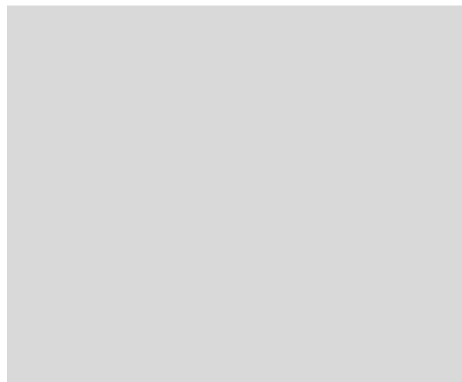

Fig. S8 Relationship of high resistance state (HRS)/low resistance state (LRS) between device area. The resistive switching mechanisms of memristor is usually dominated by conductive filaments and interfacial barrier. The resistance value in low resistance state almost does not change with increasing the device area, indicating that the main resistive switching mechanisms of the device is a local conductive filament rather than an interface barrier [17, 18].

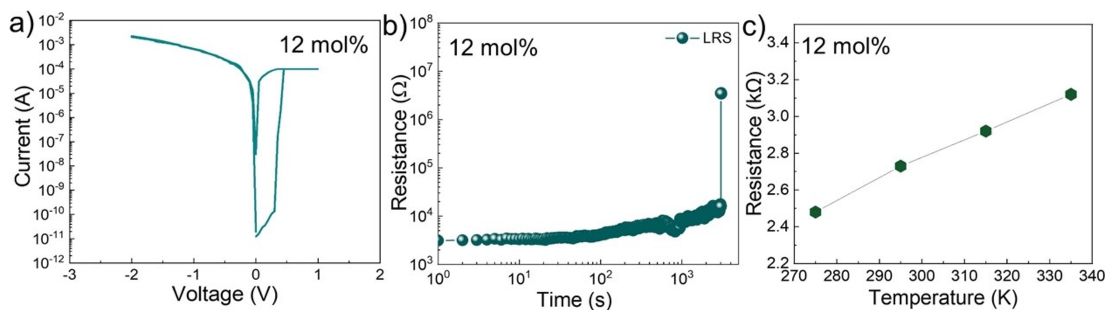

Fig. S9 a) The write-once-read-many-times behavior of device with 12 mol% Ag^+ ions doping concentration; b) The retention of low resistance state of device with 12 mol% Ag^+ ions doping concentration; c) The positive temperature dependence of the low resistance state. Compared with TS behavior of device with the lower of Ag^+ doping concentration (6 mol%), the write-once-read-many-times behavior of device with the higher of Ag^+ doping concentration (12 mol%) indicate that Ag^+ ion plays a crucial role in the resistive switching process. The temperature coefficient of resistance

under low resistance state is $4.2\times10^{-3}K^{-1}$, which was computed by $R_T = R_0[1+\alpha(T-T_0)]$[19, 20], where R_T and R_0 are the resistances at temperature T and T_0, respectively. The temperature coefficient of resistance under low resistance state is $4.2\times10^{-3}K^{-1}$, which aligns with the reported value of the Ag conductive filament [19, 20], implying that the resistance switching behavior of the device (12 mol%) can be attributed to the Ag conductive filaments mechanism.

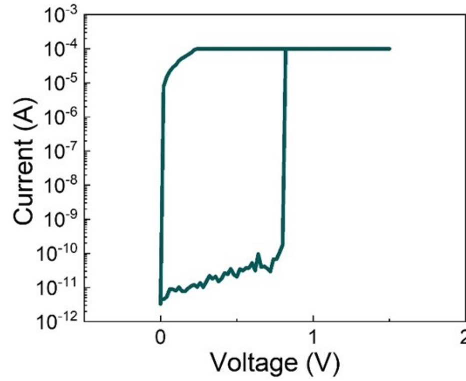

Fig. S10 The I-V curve of Ag/PMMA/OIHP/ITO device without doping Ag^+ ions.

Equation S1

The optical band gap values were obtained by Tauc's equation[21]

$$(\alpha hv)^{1/n} = B(hv - E_g) \quad \text{(S1)}$$

α is the absorption coefficient, B is the constant, hv is the photon energy, h is the Planck constant =$4.1356676969\times10^{-15}$ eV·s, v is the incident photon frequency, E_g represents the semiconductor bandgap width.

In line with previous reports[22-24], the halide perovskite is regarded as a direct-bandgap semiconductor when analyzing the optical absorption spectra (n=1/2).

Note 1 (Equation S2-S4)

$$J_s = -\left(\frac{D_s \gamma \delta^4}{KT}\right)\nabla_s K_r \quad \text{(S2)}$$

$$K_r = 1/r_1 + 1/r_2 \quad \text{(S3)}$$

$$D_s = D_s^{'} exp(-E/KT) \quad \text{(S4)}$$

Where K and T are the Boltzmann's constant and temperature; γ and δ are the surface energy and interatomic distance; K_r is surface curvature, which can be determined by the principal radii of the curvature (r_1 and r_2), the surface chemical

potential is proportional to the K_r; D_s is the diffusion coefficient, which can be determined by the diffusion coefficient pre-factor $D_s^{'}$ and the diffusion barrier E[25-28]. The limited silver content and lower I_{CC} contribute to the formation of a thinly conducting filament with a smaller radius. According to the Equation S2-S3, the J_s grows up as the radius of the filament is reduced. Due to the inherent soft lattice characteristics of halide perovskite materials, ions or atoms can readily diffuse with a larger diffusion coefficient within the halide perovskite film, also resulting in a larger J_s. Due to the higher Js value, the Ag conductive filament is prone to rapid rupture in thinnest regions.

References

1. Y. Cao, S. Wang, R. Wang, Y. Xin, Y. Peng, J. Sun, M. Yang, X. Ma, L. Lv, H. Wang and Y. Hao, *Sci China Mater*, 2023, **66**, 1569-1577.
2. X. Han, Y. Xu, B. Sun, R. Xu, J. Xu, W. Hong, Z. Fu, H. Zhu, X. Sun, J. Chang and K. Qian, *Appl. Phys. Lett.*, 2022, **120**, 094103.
3. Q. Xia, Y. Qin, P. Qiu, A. Zheng and X. Zhang, *J Mater Chem B*, 2022, **10**, 1991-2000.
4. M. Tu, H. Lu, S. Luo, H. Peng, S. Li, Y. Ke, S. Yuan, W. Huang, W. Jie and J. Hao, *ACS Appl Mater Inter*, 2020, **12**, 24133-24140.
5. G. Du, C. Wang, H. Li, Q. Mao and Z. Ji, *AIP Advances*, 2016, **6**, 085316.
6. S. Samanta, K. Z. Han, S. Das and X. Gong, *IEEE Electron Device Lett.*, 2020, **4**, 924.
7. Y. Zhou, Z. T. Song, M. Zhu, H. Huang, J. Han, K. G. Chen, C. Ye, Z. Xu, S. H. Liang, W. Xiong and X. Chen, *Volume* 2019, **7**, 1125-1128.
8. H. Y. Li, X. D. Huang, J. H. Yuan, Y. F. Lu, T. Q. Wan, Y. Li, K. H. Xue, Y. H. He, M. Xu, H. Tong and X. S. Miao, *Adv. Electron. Mater.*, 2020, **6**, 2000309.
9. Q. Luo, X. M. Zhang, J. Yu, W. Wang, T. C. Gong, X. X. Xu, J. H. Yin, P. Yuan, L. Tai, D. Dong, H. B. Lv, S. B. Long, Q. Liu and M. Liu, *IEEE Electron Device Lett.*, 2019, **40**, 718-721.
10. T. Liu, M. Verma, Y. Kang and M. Orlowski, *Appl. Phys. Lett.*, 2012, **101**, 073510.
11. D. Liu, H. Cheng, G. Wang, X. Zhu and N. Wang, *J. Appl. Phys.*, 2013, **114**, 154906.
12. T. H. Lee, D. Y. Kang and T. G. Kim, *ACS Appl Mater Inter*, 2018, **10**, 33768-33772.
13. M. C. Sahu, A. K. Jena, S. K. Mallik, S. Roy, S. Sahoo, R. S. Ajimsha, P. Misra and S. Sahoo, *ACS Appl Mater Inter*, 2023, **15**, 25713-25725.
14. J. H. Yang, S. C. Mao, K. T. Chen and J. S. Chen, *Adv. Electron. Mater.*, 2022, **9**, 2201006.
15. X. Xu, E. J. Cho, L. Bekker, A. A. Talin, E. Lee, A. J. Pascall, M. A. Worsley, J. Zhou, C. C. Cook, J. D. Kuntz, S. Cho and C. A. Orme, *Advance Science* 2022, **9**, 2200629.
16. D. Wang, S. Zhao, L. Li, L. Wang, S. Cui, S. Wang, Z. Lou and G. Shen, *Adv. Funct. Mater.*, 2022, **32**, 2200241.
17. H. S. P. Wong, H.-Y. Lee, S. Yu, Y. S. Chen, Y. Wu, P.-S. Chen, B. Lee, F. T. Chen and M.-J. Tsai, *Proc. IEEE*, 2012, **100**, 1951-1970.
18. R. Ge, X. Wu, M. Kim, J. Shi, S. Sonde, L. Tao, Y. Zhang, J. C. Lee and D. Akinwande, *Nano Lett.*, 2017,

18, 434-441.
19. X. Zhao, Z. Fan, H. Xu, Z. Wang, J. Xu, J. Ma and Y. Liu, *J. Mater Chem C*, 2018, **6**, 7195-7200.
20. S. Zhu, B. Sun, G. Zhou, T. Guo, C. Ke, Y. Chen, F. Yang, Y. Zhang, J. Shao and Y. Zhao, *ACS Appl Mater Inter*, 2023, **15**, 5420-5431.
21. E. T. Salim, S. R. Shafeeq, M. J. AbdulRazzaq, M. A. Fakhri and S. C. B. Gopinath, *Surfaces and Interfaces*, 2023, **36**, 102618.
22. S. Zhou, Y. Ma, G. Zhou, X. Xu, M. Qin, Y. Li, Y.-J. Hsu, H. Hu, G. Li, N. Zhao, J. Xu and X. Lu, *ACS Energy Letters*, 2019, **4**, 534-541.
23. H. Patil, H. Kim, K. D. Kadam, S. Rehman, S. A. Patil, J. Aziz, T. D. Dongale, Z. Ali Sheikh, M. Khalid Rahmani, M. F. Khan and D. K. Kim, *ACS Appl Mater Inter*, 2023, **15**, 13238-13248.
24. U. Das, A. Nyayban, B. Paul, A. Barman, P. Sarkar and A. Roy, *ACS Appl. Electron. Mater.*, 2020, **2**, 1343-1351.
25. W. Wang, M. Laudato, E. Ambrosi, A. Bricalli, E. Covi, Y. H. Lin and D. Ielmini, *IEEE Trans. Electron Devices*, 2019, **66**, 3795-3801.
26. W. Wang, M. Laudato, E. Ambrosi, A. Bricalli, E. Covi, Y. H. Lin and D. Ielmini, *IEEE Trans. Electron Devices*, 2019, **66**, 3802-3808.
27. W. Wang, M. Wang, E. Ambrosi, A. Bricalli, M. Laudato, Z. Sun, X. Chen and D. Ielmini, *Nat. Commun.*, 2019, **10**, 81.
28. J. Sun, L. He, Y. C. Lo, T. Xu, H. Bi, L. Sun, Z. Zhang, S. X. Mao and J. Li, *Nat. Mater*, 2014, **13**, 1007-1012.